Earth Planets Space, **59**, 1211–1217, 2007

Two-dimensional resistivity structure of the fault associated with the 2000 Western Tottori earthquake

Satoru Yamaguchi[1], Hideki Murakami[2], Hisanori Iwamoto[3], Kazuhiro Takemoto[3], Kazuya Kitada[3], Ichiro Shiozaki[4], Naoto Oshiman[5], and Shigehiro Katoh[6]

[1]*Department of Earth and Planetary Sciences, Faculty of Science, Kobe University, Nada, Kobe 657-8501, Japan*
[2]*Faculty of Science, Kochi University, Akebono-cho, Kochi, Japan*
[3]*Graduate School of Science and Technology, Kobe University, Kobe, Japan*
[4]*Faculty of Engineering, Tottori University, Koyama-minami, Tottori, Japan*
[5]*Disaster Preventions Research Institute, Kyoto University, Kyoto, Japan*
[6]*Museum of Nature and Human Activities, Hyogo Prefecture, Japan*

(Received August 30, 2006; Revised October 12, 2007; Accepted November 6, 2007; Online published January 11, 2008)

Two-dimensional resistivity surveys were carried out along two profiles that were laid across earthquake faults initiated by the 2000 Western Tottori earthquake. One profile was located 7 m from a trenching pit, thereby enabling a direct comparison of resistivity cross-section with the geological cross-section and, subsequently, a precise interpretation of the resistivity structure. Features of the resistivity cross-section were found to correspond fairly well to the geological cross-section. A clear resistivity boundary between the resistive and conductive zones matches the earthquake fault that was found by the trenching survey. Variations in resistivity depend primarily on the development of fractures. Two types of conductive zones were found: (1) a clear and deep-rooted conductor that corresponds to an earthquake fault and (2) an indistinct and spatially localized conductor that corresponds to a fracture attributed by landslides and collapse. A few weak conductive zones that match with discrete earthquake faults characterize our resistivity model. This feature is different from the resistivity cross-sections found at the Nojima and Ogura Faults that appeared at the time of the 1995 Hyogo-ken Nanbu earthquake; these two latter faults are characterized by distinct single conductive zones. Based on geomorphological, geological, and seismological evidence, the earthquake fault of the 2000 Western Tottori earthquake can be classified as an immature fault. In contrast, the Nojima and Ogura Faults have been active for at least the entire Quaternary period. We conclude that the difference in the fault development stages is reflected in their different resistivity structures.

Key words: The 2000 Western Tottori Earthquake, resistivity structure, 2-D resistivity survey, active fault, fault maturity.

1. Introduction

Electrical (DC) resistivity surveys and magnetotelluric surveys commonly reveal changes in apparent resistivity and/or phase value across the surface trace of an active fault. A clearly distinguishable low resistive zone (sometimes called the fault zone conductor (FZC)) has been found along a fault trace at many faults throughout the world (see Electromagnetic Research Group for the Active Fault (ERGAF), 1982; Unsworth *et al*., 1997). The conductor is basically caused by a fluid network distributed within a fracture zone along the fault (ERGAF, 1982; Ritter *et al*., 2005). The FZC image varies with the pattern of fault activity and the stage of the fault development. For example, different FZCs have been imaged along a locked segment and a creep segment (Unsworth *et al*., 1999). Yamaguchi *et al*. (2001, 2002) reported that during the 1995 Hyogo-ken Nanbu earthquake (the 1995 Kobe earthquake) there were differences in the FZC image between a segment where a large displacement was observed and a segment where little displacement was observed. This difference clearly illustrates that electrical resistivity structure is one of the important parameters that characterize an active fault.

The 2000 Western Tottori earthquake occurred on 6 October 2000, with the epicenter in the western part of Tottori Prefecture, Chugoku district, southwestern Honshu, Japan (Fig. 1(b)). The magnitude of the main shock was 7.3, and the focal depth was 11 km (Japan Meteorological Agency, JMA). The aftershock area of this earthquake is shown in Fig. 1(a). Swarm activities had been observed in the western part of Tottori Prefecture prior to the earthquake, but there was no indication of an active surface fault corresponding to these earthquakes. Since the earthquake, many detailed field surveys have been carried out in the aftershock area. Fusejima *et al*. (2001) found five surface fractures along NW-SE trending lines in an area 6 km long and 1 km wide. Inoue *et al*. (2002) also found some NW-SE trending lineaments with a sinistral offset of valleys and ridges based on aerial photograph interpretation, geological inves-

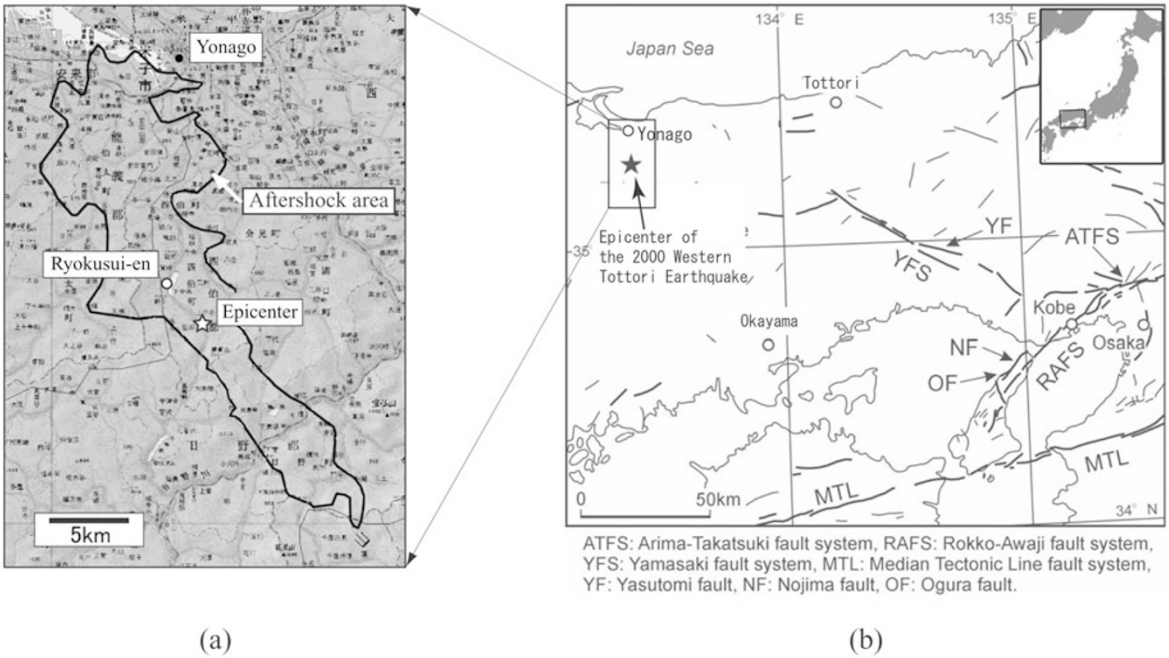

Fig. 1. (a) Survey point of this study and aftershock area of the 2000 Western Tottori earthquake. Black line encloses aftershock area of the 2000 Western Tottori earthquake. Star shows epicenter of the 2000 Western Tottori earthquake. (b) Distribution of active faults in the western part of the Kinki district and in the eastern part of the Chugoku district, Japan. Traces of active faults are modified after Research Group for Active Faults of Japan (1991).

tigations and trenching studies in the aftershock zone. In both studies, these lineaments were interpreted as active faults because fault gouge and horizontal striations on sharp fault planes were found along the lineaments. Some of these were recognized to be initiated by the 2000 Western Tottori earthquake. However, the fault length of these earthquake faults (about 6 km) is significantly shorter than the expected length (about 30 km) calculated using the empirical law between the magnitude of an earthquake and the length of the earthquake fault (Matsuda, 1975). The fracture zones along the earthquake faults in the aftershock area have quite poor fault gouge belts and no cataclasite zones (Fusejima *et al*., 2002). Inoue *et al*. (2002) stated strongly that these are immature faults based on the short fault lengths with narrow fracture zones. Their assessment is supported by the results of seismological studies that also suggest the immaturity of these faults. The aftershocks of the earthquake resulted in some clusters, especially in the northern part of the aftershock area (e.g. Katao and Yoshii, 2002). Fukuyama *et al*. (2003) resolved detailed fault structures activated by the main shock of the 2000 Western Tottori earthquake. Their estimated fault model consists of four fault planes in the southern area up to a scattering of eight fault planes in the northern area. This model shows that this earthquake fault, which was first observed at the time of the 2000 Western Tottori earthquake, is at an initial stage of fault development.

Many FZC imaging studies have been carried out on mature faults, such as the San Andreas Fault (Unsworth *et al*., 1997, 1999; Bedrosian *et al*., 2002, 2004) and the West Fault in northern Chile (Janssen *et al*., 2002), or for ceased faults (Yamaguchi *et al*., 2002). Few FCZ studies have been carried out for faults at an initial stage of development.

In this paper, we present resistivity models based on the results of two-dimensional resistivity surveys along two profiles crossing the earthquake fault that were carried out to determine the subsurface resistivity structure of the fault. These models are interpreted in detail following a comparison of the results with those of a trenching survey that was conducted only 7 m away from one of our profiles. We also compare the resistivity structure beneath the earthquake fault from the 2000 Western Tottori earthquake and those from the 1995 Hyogo-ken Nanbu earthquake and discuss resistivity structures at different stages of fault development.

2. Observations

The profiles of two-dimensional resistivity surveys were laid across the surface ruptures in the grounds of the Ryokusui-en (Fig. 2), which is a lodge located in the center of the aftershock zone (Fig. 1(a)). Fusejima *et al*. (2001) found a ten-centimeter sinistral offset of a road and a gutter line along the surface rupture near the Ryokusui-en lodge.

The first observation along Profile-1 was made in December 2001, and the second observation, along Profile-2, was carried out in April 2002. The direction of Profile-1 is N33°E–S33°W, which is perpendicular to the strike of the surface ruptures. The total length of the profile was 31 m, and the center of the profile was fixed on the rupture. Thirty-two electrodes were installed along the profile at a spacing of 1 m. Profile-2, which had a total length of 63 m, was laid parallel to Profile-1 at a distance of 3 m towards the southeast; 64 electrodes were installed at 1-m intervals.

Resistivity surveys of two different configurations, Wenner and Eltran configurations, were conducted along the two profiles using a McOHM21 system (OYO Corporation,

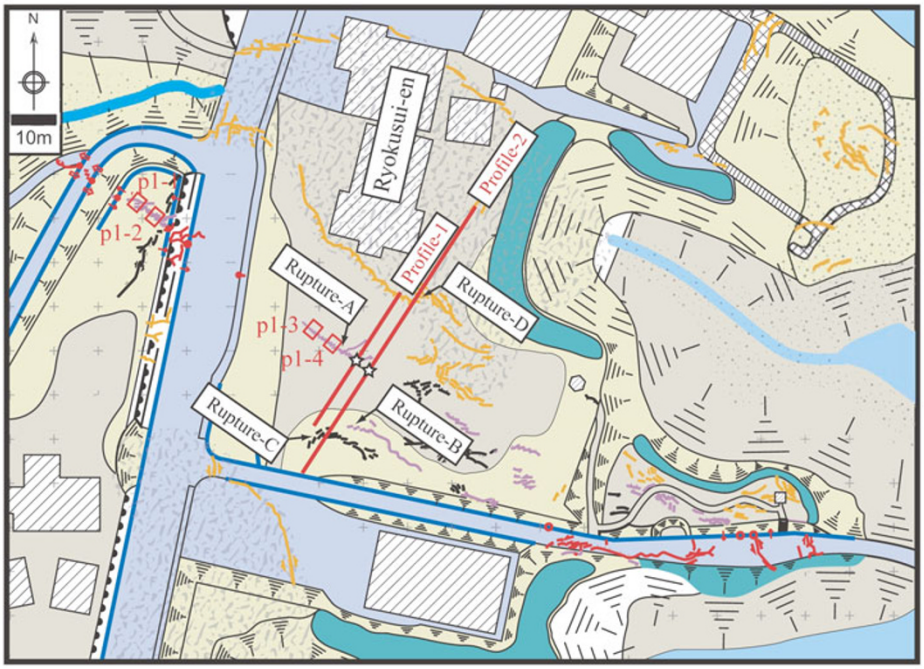

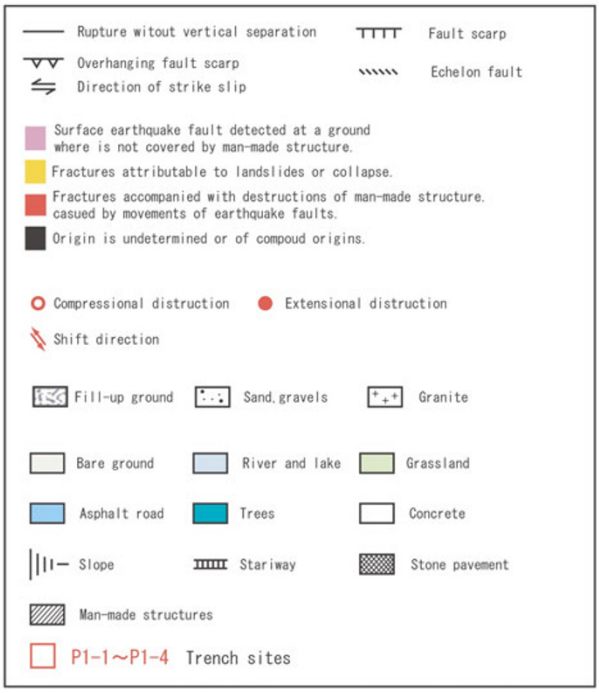

Fig. 2. Profiles for the 2-dimensional (2-D) resistivity surveys. Two profiles of the resistivity surveys (Profile-1 and Profile-2) are laid on the detailed map showing the result of the geological investigation at the Ryokusui-en by Fusejima *et al*. (2001). Red squares labeled p1-1～p1-4 show trench sites of Fusejima *et al*. (2002). Profile-1 crosses Rupture-A, which was studied by a trenching survey. Stars on these lines show the location of 27 m along the profile. P1-1, p1-2, p1-3 and p1-4 indicate trench sites of Fusejima *et al*. (2002).

Japan). The apparent resistivity at each measurement point was taken five times, and the mean value with a standard deviation was adopted as the representative value and error at that point.

3. Model Analysis

Two-dimensional (2-D) inversions were made using a code for the smoothness-constrained inversions for DC resistivity data with an Akaike's Bayesian Information Criterion (ABIC) minimization method (Uchida, 1993). The starting model was a 100 Ω m uniform halfspace with topography for both profiles. After 20 iterations, the ABIC minimum model was adopted as the most plausible one.

3.1 Profile-1

The final model of Profile-1 (Model 1) is shown in Fig. 3(b). The forward response of Model 1 explains the

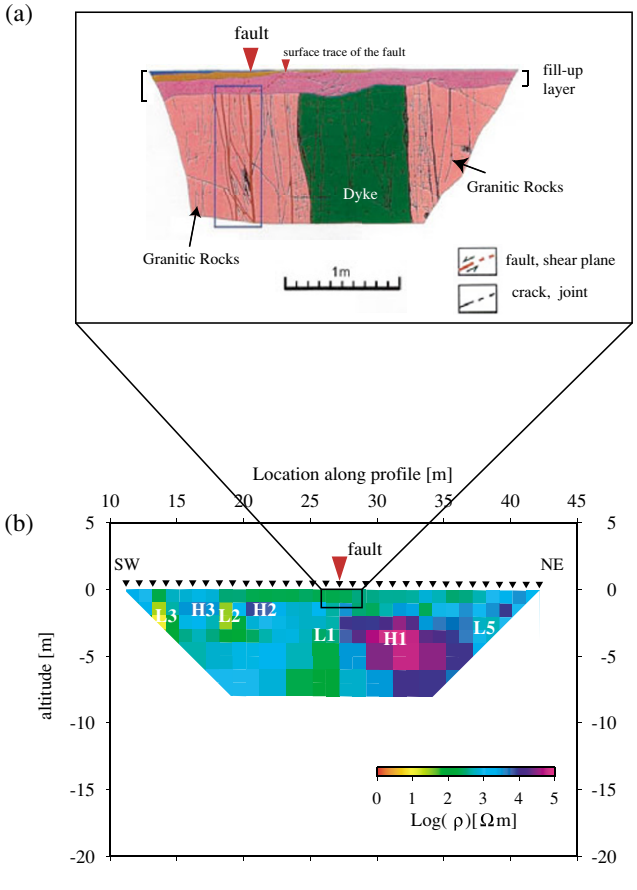

Fig. 3. Final two-dimensional resistivity model along Profile-1 (Model-1) with the geological cross-section. (a) Sketch of the northwestern wall of P1-4. This figure was drawn from figure 7 of Fusejima *et al.* (2002). A large closed red reversed triangle shows the location of the earthquake fault. A small closed red reversed triangle shows the surface trace of the earthquake fault, and this location corresponds to the star mark on Profile-1 in Fig. 2. (b) Two-dimensional resistivity cross-section along Profile-1. A closed red reversed triangle shows the location of Rupture-A. Black reversed triangles show location of the electrodes. A solid line encloses the area of the trenching survey by Fusejima *et al.* (2001).

observed values well (Fig. 4). The normalized root mean square (r.m.s.) misfit between the model and the observed values was 1.01.

The model is characterized by three resistive (H1, H2 and H3) and four conductive (L1, L2, L3 and L5) zones. Highly resistive zone H1 (>20,000 Ω m) is found below a depth of 2 m at between 27 m and 37 m on the profile. Conductive zone L1 exists adjacent to the highly resistive zone H1. This conductive zone is a few meters wide, and its resistivity is less than 200 Ω m below a depth of 4 m. The boundary between these two zones (H1 and L1) does not reach the surface, but is clearly visible below a depth of 1 m. Two other resistive and three conductive zones are also recognizable, but these are smaller than zones H1 and L1 and are localized spatially. The top-most layer, which is about 1 m thick, lies on these resistive and conductive zones.

3.2 Profile-2

The final model of Profile-2 (Model 2) is shown in Fig. 5. The forward response of Model 2 also explains the observed values well (Fig. 6). The r.m.s. misfit was 1.01.

The model is characterized by six resistive (H1–H6) and six conductive (L1–L6) zones. Three resistive zones (H1, H2, and H3) and four conductive zones (L1, L2, L3, and L5) are commonly found in the area which overlaps the area of Model 1, and we assigned the same numbers to both models. Two resistive zones, H1 and H6, have a high resistivity of 20,000 and 10,000 Ω m, respectively, and seem to be rooted at a depth beyond the limit of our observation. The other resistive zones (H2–H5) are small and spatially localized. Their maximum resistivities are a few thousand ohm-meters. Conductive zone L1 seems to be less clear and smaller than its counterpart of Model 1. Zones L3 and L4 are remarkably conductive, and their resistivities are a few tens of ohm-meters, which is less than the resistivity of L1 in Model 2; the top-most layer, which is about 1 m thick, lies on these resistive and conductive zones as for Model 1.

4. Discussion

We interpreted Model 1 by comparing the results obtained in this study with those of the trenching survey carried out by Fusejima *et al.* (2002) (Fig. 3). Trench sites were located at and near the Ryokusui-en lodge (p1-1, p1-2, p1-3, and p1-4 in Fig. 2). Profile-1 is located only 7 m away from pit p1-4. Figure 3(a) shows the northwestern wall of p1-4. Granitic rocks and an intrusive dyke of a porphyritic nature exist under the fill-up layer (20–30 cm thick at these sites). Shear zones are recognized in both the granitic rocks and the dyke, but they are better developed in the granitic rocks (especially in the blue box in Fig. 3(a)). The shear zone has a similar strike (N40°W) to that of the earthquake fault and consists of parallel shear planes with a fault gouge and planer fabrics.

The clear boundary between high and low resistive zones at 27 m on the profile corresponds to the earthquake fault (a closed red reversed triangle in Fig. 3). The highly resistive zone H1 corresponds to both granite and an intrusive dyke that are less fractured (Fusejima *et al.*, 2002). The dyke is too narrow (<1 m) to explain solely this highly resistive zone. The shear zone corresponds to the upper extent of the conductive zone L1. It is worth noting that the variation in resistivity does not correspond to the lithology (granite or dyke) but, rather, to the development of fractures. The dyke could, however, serve as a permeability barrier to fluid flow within well-fractured granite. In addition, two resistive (H2 and H3) and three conductive (L2, L3, and L5) zones are found. These were interpreted as less-fractured and better-fractured granites, respectively. The top-most uniform layer indicates an artificial fill-up layer.

The corresponding area in Model 2 (the trapezoid area in Fig. 5) has a structure similar to that in Model 1. The highly resistive zone H1 and conductive zone L1 and the topmost uniform layer in Model 2 are interpreted to be the same as those in Model 1. A 3-m shift of the resistivity boundary to the northeast is consistent with the change in the trend of the surface trace of the earthquake fault from NW-SE to NE-SW (Rupture-A in Fig. 2). The conductive zone L1 seems to be less dinstint than that in Model 1, possibly because Profile-2 lay near the southeastern terminal of the surface trace of the earthquake fault. The clear conductive zone L3 is recognized at 16 m along the profile. It is wider

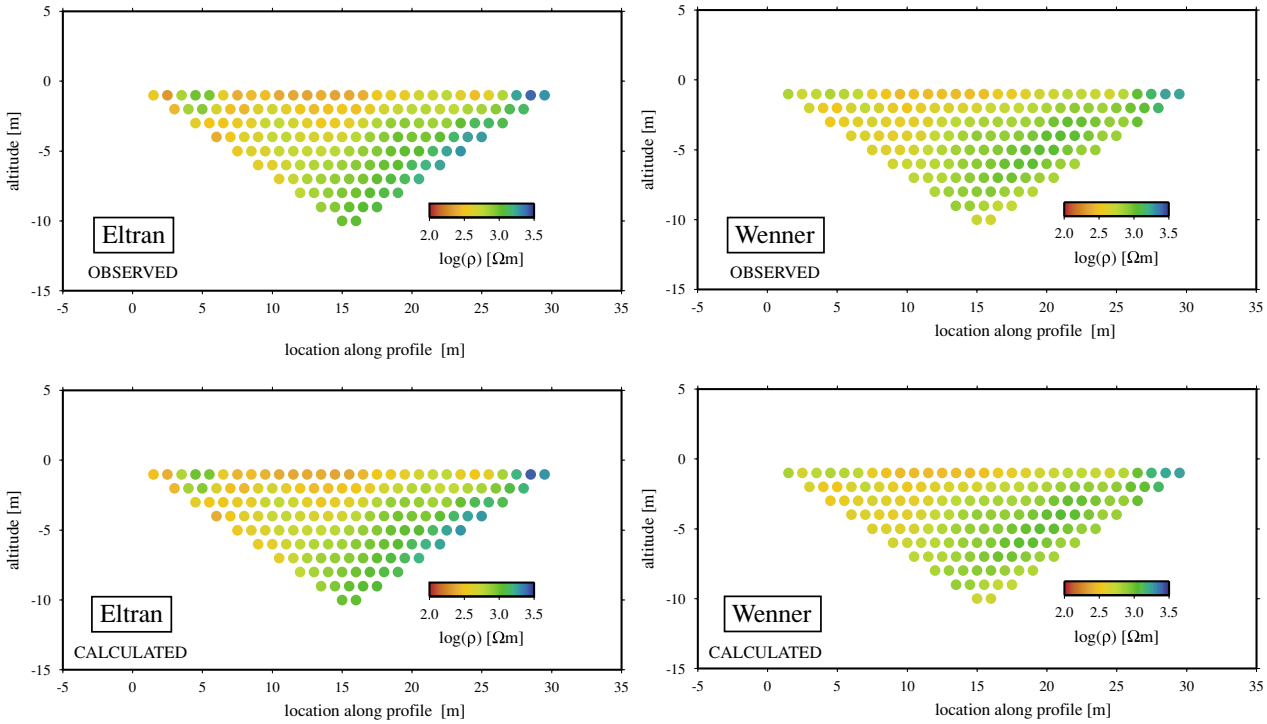

Fig. 4. Comparison of the forward responses of Model 1 and the observed values along Profile-1. Left panels indicate observed data (upper panel) and forward responses of Model 1 (lower panel) for the Eltran configuration. Right panels indicate those for the Wenner configuration.

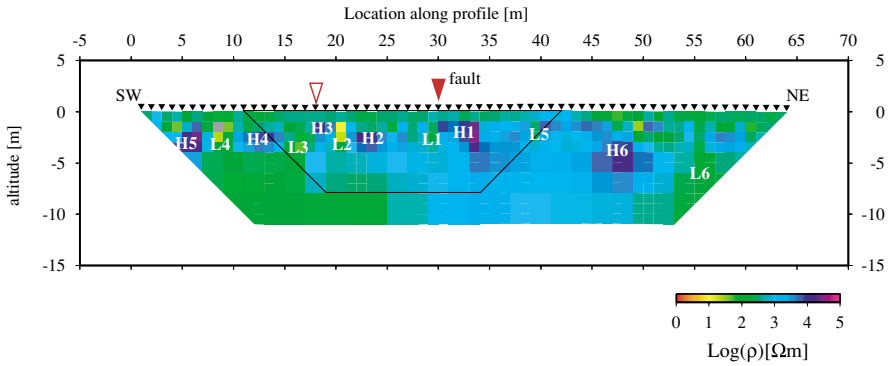

Fig. 5. Final two-dimensional resistivity model along Profile-2 (Model 2). Black reversed triangles indicate the location of the electrodes. A closed red reversed triangle shows the location of Rupture-A and an open red reversed triangle shows the location of Rupture-B. The black trapezoid indicates the area of Model 1. Gray cells show the cell with less reliable resistivity. A cell with resistivity different from that of the surrounding eight cells by more than one order was defined as an anomalous cell.

and more conductive (the minimum resistivity is less than 50 Ω m) than conductive zone L1. Furthermore, a boundary between L3 and H3 (an open red reversed triangle in Fig. 5) corresponds to the southwestern extent of the earthquake fault (Rupture-B in Fig. 2). Beyond the area of Model 1, three resistive zones (H4, H5 and H6) and a conductive zone (L4) are depicted. The resistive zone H6 is as large as that of zone H1 and deep-rooted. It may be composed of less-fractured granites because it is connected to zone H1 by the small conductive zone L5. Three conductive zones (L3, L4 and L5) can be classified into two groups: zones L3 and L4, and zone L5. Both zones L3 and L4 are deep-rooted and highly conductive. The width of L4 is about 3 m and the resistivity is almost the same as that of L3. This zone corresponds to Rupture-C (Fig. 2), and its origin is classified as 'undetermined or of compound origin' (Fusejima *et al.*, 2001). As zone L4 has features similar to those of zones L1 and L3, the origin of this zone is judged to be same as zones L1 and L3, that is, Rupture-C is an earthquake fault. In contrast, zone L5 corresponds to Rupture-D, which is classified as attributable to 'landslide and collapse'. The resistivity structure of zone L5 is more localized and less distinct than those of zones L1 and L3. Based on these results, we may say that a high-resolution 2-D resistivity survey is a useful approach to detect an earthquake fault even though it is unclear on the ground.

The 1995 Kobe earthquake, a shallow inland earthquake in southwestern Japan, was also a large earthquake with a magnitude of more than 7.0. During the Kobe earthquake, distinctive fault ruptures appeared along the Nojima and the Ogura Faults (NF and OF in Fig. 1(b)). Scientists were

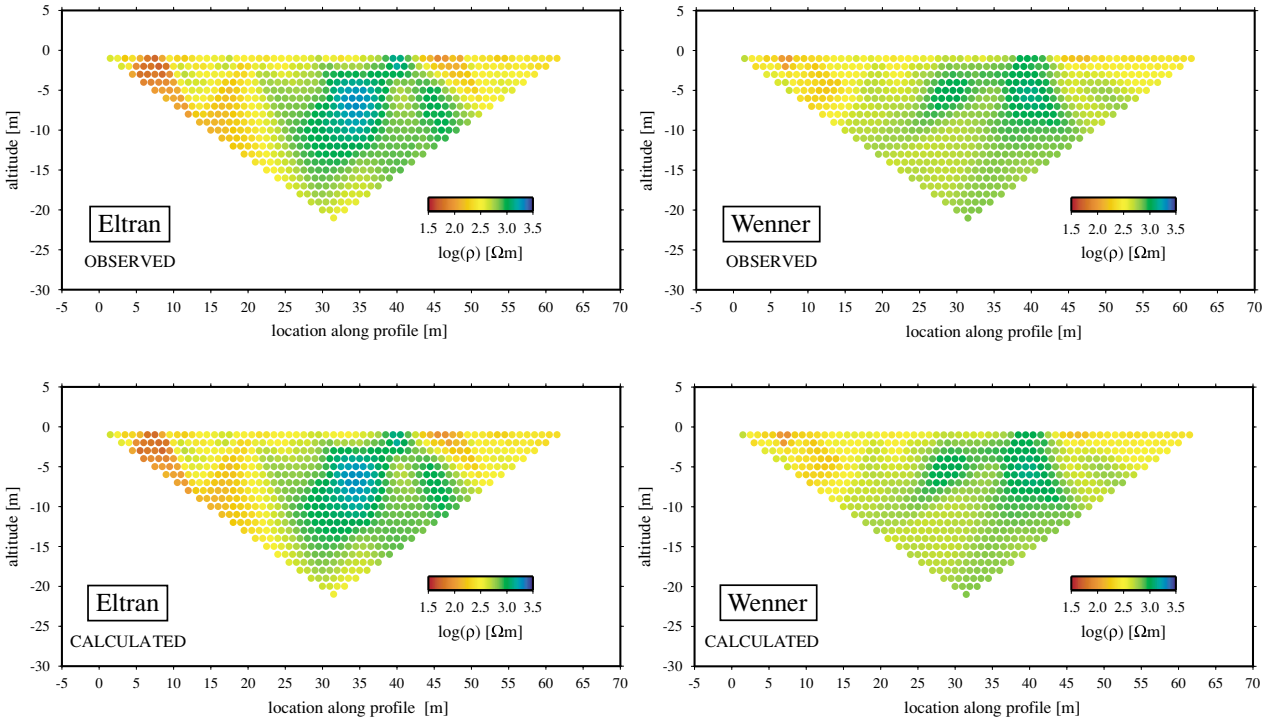

Fig. 6. Comparison of the forward responses of Model 2 and the observed values along Profile-2. Left panels indicate observed data (upper panel) and forward responses of Model 2 (lower panel) for the Eltran configuration. Right panels indicate those for the Wenner configuration.

aware of the Nojima Fault prior to the 1995 Kobe earthquake. The fault ruptures that appeared during the 1995 Kobe earthquake differ greatly from those appearing in the 2000 Western Tottori earthquake even those two earthquakes occurred in a similar tectonic setting: in the former, distinctive fault ruptures appeared along a pre-existing fault. The Nojima and Ogura Faults consist of a southwestern segment of the Rokko-Awaji Fault system (Fig. 1(b)) with a total length of nearly 60 km, and they have been active for at least the entire Quaternary (e.g. Nakata and Okada, 1999). Two-dimensional resistivity surveys revealed distinct, single and wide conductive zones at six sites along the faults (Koreishi *et al*., 1996; Takahashi *et al*., 1996). The conductive zones of these studies are much wider (5 m to some tens of meters) than that found by this study. It is worth noting that these studies provide good comparisons with our results of our study because the resistivity models were obtained by the same method and have the same spatial resolution.

We have compared the fault resistivity structure of the 2000 Western Tottori earthquake with that of the 1995 Kobe earthquake. Two weak conductive zones (L1 and L3) were depicted where there were earthquake faults from the 2000 Western Tottori earthquake. This feature is different from resistivity cross-sections at the Nojima and Ogura Faults. The fault of the 2000 Western Tottori earthquake is recognized as an immature fault based on geomorphological, geological and seismological evidence. In contrast, the Nojima and Ogura Faults have been active for at least the entire Quaternary. We suggest that the different resistivity structure reflects the different stage of fault development. Inoue *et al*. (2002) pointed out that the distribution pattern of lineaments in the epicentral area of the 2000 Western Tottori earthquake is similar to the distribution pattern at the initial stage of fault development for the sandbox experiment (Ueta *et al*., 2000). Ueta *et al*. (2000) showed, for a sinistral case, that right-stepping shears develop on both sides of the basement fault at the initial stage, with only small displacement, and that short-length shears develop discretely near the fault at this stage. As the basement displacement increases, shears on both sides of the basement fault join together to form a helicoidal shape. Finally, a long straight fault is formed as a principal displacement shear. Fluids and/or clay distributed within the fracture network of the shear zone form weak and discrete low resistivity zones during the initial stage of fault development. These are subsequently transformed to a wide and distinct conductive zone along a fault during the final stage.

Acknowledgments. We wish to thank Dr. Yuichiro Fusejima (GSJ, AIST) for his helpful discussion on fault ruptures and results of the trenching surveys. We are thankful to the staff members of the Ryokusui-en lodge for their support during our measurements on their property. We thank P. A. Bedrosian and an anonymous reviewer for their critical and constructive comments, which have helped to improve this manuscript. This study was financially supported by the Joint Research Project (Exploratory Subject: 13H-3) of Disaster Prevention Research Institute, Kyoto University. The Research Center for Urban Safety and Security (Kobe University) financially supported this work and allowed us to use the McOHM21 instrument. Many of the figures in the manuscript were drawn using Generic Mapping Tools (Wessel and Smith, 1998).

References

Bedrosian, P. A., M. J. Unsworth, and G. Egbert, Magnetotelluric imaging of the creeping segment of the San Andreas Fault near Hollister, *Geophys. Res. Lett*., **29**, doi 10.1029/2001GL014119, 2002.

Bedrosian, P. A., M. J. Unsworth, G. D. Egbert, and C. H. Thurber, Geophysical images of the creeping segment of the San Andreas fault: impli-

cations for the role of crustal fluids in the earthquake process, *Tectonophysics*, **385**, 137–158, 2004.

Electromagnetic Research Group for the Active Fault, Low electrical resistivity along an active fault, the Yamasaki fault, *J. Geomag. Geoelectr.*, **34**, 103–127, 1982.

Fukuyama, E., W. L. Ellsworth, F. Waldhauser, and A. Kubo, Detailed fault structure of the 2000 Western Tottori, Japan, earthquake sequence, *Bull. Seismol. Soc. Am.*, **93**, 1468–1478, 2003.

Fusejima, Y., T. Yoshioka, K. Mizuno, M. Shishikura, R. Imura, T. Komataubara, and T. Sasaki, Surface ruptures associated with the 2000 Tottori-ken Seibu earthquake, *Annu. report on active fault and paleoearthquake researches*, **1**, 1–26, 2001 (in Japanese with English abstract).

Fusejima, Y., R. Imura, M. Morino, Y. Sugiyama, and K. Mizuno, Trenching surveys of surface ruptures associated with the 2000 Tottori-ken-seibu earthquake, *Annu. report on active fault and paleoearthquake researches*, **2**, 183–208, 2002 (in Japanese with English abstract).

Inoue, D., K. Miyakoshi, K. Ueta, A. Miyawaki, and K. Matsuura, Active fault study in the 2000 Tottori-ken seibu earthquake area, *Zisin (J. Seismol. Soc. Jpn.)*, **54**, 557–573, 2002 (in Japanese with English abstract).

Janssen, C., A. Hoffmann-Rothe, S. Tauber, and H. Wilke, Internal structure of the Precordilleran fault system (Chilie)—insights from structural and geophysical observations, *J. Struc. Geol.*, **24**, 123–143, 2002.

Katao, H. and K. Yoshii, The aftershock distribution derived from the urgent observations just after the Western Tottori Prefecture earthquake in 2000, *Zisin (J. Seismol. Soc. Jpn.)*, **54**, 581–585, 2002 (in Japanese).

Koreishi, Y., J. Fujita, H. Nakahigashi, S. Asakawa, S. Senna, and K. Ishigaki, The geophysical characteristics of active faults in Hanshin district, *Butsuri-Tansa*, **49**, 487–497, 1996 (in Japanese with English abstract).

Matsuda, T., Magnitude and recurrence interval of earthquakes from a fault, *Zisin II*, **28**, 269–284, 1975 (in Japanese with English abstract).

Nakata, T. and A. Okada (ed.), *Nojima Fault: Pictorial Record and Explanatory Text*, 208 pp., University of Tokyo Press, Tokyo, 1999 (in Japanese).

Research Group for Active Faults of Japan (ed.), *Active Faults in Japan (sheet maps and inventories)*, 437 pp., University of Tokyo Press, Tokyo, 1991 (in Japanese with English abstract).

Ritter, O., A. Hoffmann-Rothe, P. A. Bedrosian, U. Weckmann, and V. Haak, Electrical conductivity images of active and fossil fault zones, 165–186, in *High-strain Zones: Structure and Physical Properties*, GSA Special Publication 245, 2005.

Takahashi, T., K. Nozaki, H. Shima, M. Yamane, and T. Igarashi, Field experiments of various geophysical methods at the Nojima fault, *Butsuri-Tansa*, **49**, 498–510, 1996 (in Japanese with English abstract).

Uchida, T., Smoothness-constrained 2D inversion for DC resistivity data by ABIC minimization method, *Butsuri-Tansa*, **46**, 105–119, 1993.

Ueta, K., K. Tani, and T. Kato, Computerized X-ray tomography analysis of three-dimensional fault geometries in basement-induced wrench faulting, *Eng. Geol.*, **56**, 197–210, 2000.

Unsworth, M. J., P. E. Malin, G. D. Egbert, and J. R. Booker, Internal structure of the San Andreas fault at Parkfield, California, *Geology*, **25**, 359–362, 1997.

Unsworth, M., G. Egbert, and J. Booker, High-resolution electromagnetic imaging of the San Andreas fault in Central California, *J. Geophys. Res.*, **104**, 1131–1150, 1999.

Wessel, P. and W. H. F. Smith, New, improved version of generic mapping tools released, *EOS Trans. AGU*, **79**, 579, 1998.

Yamaguchi, S., T. Murakami, and H. Inokuchi, Resistivity mapping using the VLF-MT method around surface fault ruptures on the 1995 Hyogo-ken Nanbu earthquake, Japan, *The Island Arc*, **10**, 296–305, 2001.

Yamaguchi, S., S. Sutoh, T. Hashimoto, H. Murakami, and N. Takagi, 2-D resistivity structure of the southern part of the Nojima fault and relationship to the activity of the faults, *Zisin (J. Seismol. Soc. Jpn.)*, **55**, 143–151, 2002 (in Japanese with English abstract).

S. Yamaguchi (e-mail: yanchi@kobe-u.ac.jp), H. Murakami, H. Iwamoto, K. Takemoto, K. Kitada, I. Shiozaki, N. Oshiman, and S. Katoh